Efficiency and Power Compatibility Visualization Methodology for Dynamic Wireless Power Transfer

Ryotetsu Sakurai
Faculty of Science and Technology
Tokyo University of Science
Noda, Japan
sakurai.ryotetsu21@gmail.com

Takehiro Imura
Faculty of Science and Technology
Tokyo University of Science
Noda, Japan

Yochi Hori
Faculty of Science and Technology
Tokyo University of Science
Noda, Japan

***Abstract*— In recent years, wireless power transfer has been attracting attention as a means of improving quality of life. In particular, Wireless Power Transfer to electric vehicles is important as part of efforts to solve environmental problems because it contributes to the widespread adoption of electric vehicles. Since electric vehicles need to be recharged more frequently than conventional gasoline-powered vehicles, there are problems such as charging while parked is not enough to cover a sufficient distance, and there is not enough space to install a lot of charging station. Therefore, wireless power transfer to running electric vehicles (DWPT) is important. In this study, the method, which can visualize the compatibility is proposed. The compatibility is visualized by mapping the transfer power and efficiency corresponding to the positional relationship between the transmitting and receiving coils in a DWPT system. Proposed method can be applied not only to sine waves, but also to square waves, which are closer to the real environment. By using this method changes in those coils' positions can be taken considered easily when designing a WPT system. The proposed method is demonstrated by experiments.**

Keywords*— *Wireless Power Transfer, DWPT, Compatibility, Electric Vehicle, Power, Efficiency, Visualization

I. Introduction

Research on Wireless Power Transfer (WPT), which is the transfer of power without cables, is gaining momentum [1]. In particular, WPT for running electric vehicles (DWPT) has advantages such as enabling long-distance driving and reducing the number of charging stations [2-9]. However, it is known that in DWPT, the positional relationship between the transmitting and receiving coils constantly changes, which also changes the transfer characteristics. The power transfer characteristics of a WPT can be obtained by some method such as solving the KVL equation based on the equivalent circuit of a WPT [10], but it is difficult to analyze and clearly understand the changing transfer characteristics of a DWPT. To solve this problem, there is research on a method to visualize the compatibility of transmittable power by mapping the magnitude of the power in response to changes in the positional relationship [11,12]. However, the conventional method can only check the maximum power that can be transferred and does not correspond to the transfer efficiency. Therefore, this study proposes a method to visualize compatibility including efficiency. The compatibility is visualized by mapping the transfer power and efficiency corresponding to the positional relationship between the transmitting and receiving coils in a DWPT system. The proposed method can be applied not only to systems with sine wave inputs, but also to systems with square wave inputs that are similar to real-world environments. Chapter 2 shows the principle of the conventional impedance mapping method that visualizes only power, and Chapter 3 shows the principle of the new impedance mapping method that includes efficiency. In addition, the principle of the square wave input is also presented. Chapter 4 demonstrates the method through experiments, and Chapter 5 presents conclusions.

II. Theory of the Impedance Map for Power

The impedance mapping method already proposed to visualize the power transfer characteristics is described. Fig. 1a shows a typical WPT circuit. In Fig. 1a, Z_1 to Z_3 represent the primary resonant circuit and Z_4 to Z_6 represent the secondary resonant circuit.

Z_{ref} in Fig. 1b is the equivalent impedance reflecting the circuit configuration, coupling coefficient, and load conditions on the secondary side. If the composite impedance of the secondary side is Z_s and the mutual inductance is L_m, it can be derived as in (1).

$$Z_{ref} = \frac{(\omega L_m)^2}{Z_s} \tag{1}$$

The impedance map method creates a map with R_{ref} and X_{ref}, the real and imaginary parts of Z_{ref}, as axes. It focuses on the fact that Z_{ref} varies depending on the coupling coefficient state of the coils and load variations, and can be used to evaluate the power that can be transmitted. In Fig. 1a, the compensation circuit is configured as an LCC/LCC circuit [13], but it can be used in other circuit configurations such as S/S circuits [14,15] by setting the value of each element to 0 (short) or ∞ (open).

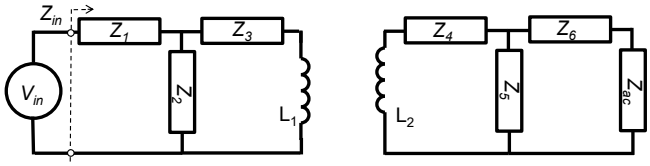

(a) WPT circuit

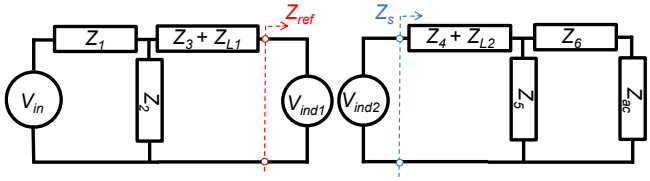

(b) Z_{ref} and Z_s on the circuit

Fig. 1. General WPT circuit

The impedance map can be created by combining the power map shown in Fig. 2a and the Z_{ref} trajectory shown in Fig. 2b. Fig. 2b shows the trajectory when the coupling coefficient is varied from 0.00319 to 0.124. The conventional impedance map was created by combining the power map and Z_{ref} trajectory and is shown in Fig. 3.

The map in Fig. 2 uses the parameters shown in Table I. A sine wave of 85 kHz is input as the power source.

The number on the line in the power map represents the amount of power that can be transferred to the secondary side. The 1,000 and 2,000 lines in Fig. 3 are cut out of the corresponding lines from Fig. 2a. The value of transferable power is determined by the inverter and coil ratings. The maximum power that can be transferred is calculated as in (2)~(4) using the rated current I_{L1max} of the transfer coil, the rated supply voltage V_{max}, and the rated supply current I_{max}.

$$P_{trans}^{L1} = R_{ref} I_{L1max}^2 \tag{2}$$

$$P_{trans}^{V} = \frac{R_{in}}{R_{in}^2 + X_{in}^2} V_{max}^2 \tag{3}$$

$$P_{trans}^{I} = R_{in} I_{max}^2 \tag{4}$$

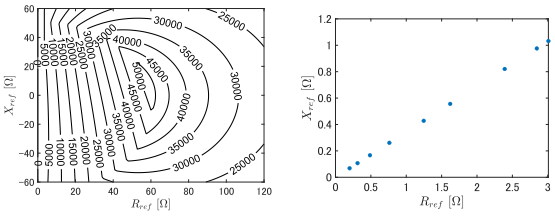

(a) Power Map (b) Z_{ref} Trajectory

Fig. 2. Power Map and Z_{ref} Trajectory

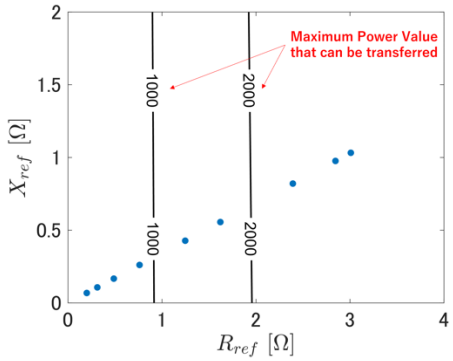

Fig. 3. Conventional Impedancemap

TABLE I. PARAMETERS OF IMPEDANCE MAP DRAWING

	R	X
L_1	0.189 Ω	128 μH
L_2	0.112 Ω	145 μH
Z_1	71.3 mΩ	28.1 μH
Z_2	39.0 mΩ	129 nF
Z_3	40.3 mΩ	36.6 nF
Z_4	3.07 Ω	27.5 nF
Z_5	0.34 Ω	91.8 nF
Z_6	28.7 mΩ	37.2 μH
Z_{ac}	10.4 Ω	--

The actual maximum power available for transfer is determined by comparing the power values obtained from (2) to (4) and the minimum of the power values. In Fig. 2(a), (2) to (4) are substituted under the conditions of 438 V rated voltage of the power supply, 120 A rated current of the power supply, and 38 A rated current of the coil [16]. In this paper, the same factors as in previous studies are considered as constraints [17]. Therefore, if there are other parameters to consider, such as coil voltage, the maximum power available for transfer should be calculated by using rating of that parameters.

The Z_{ref} trajectory shown in Fig. 2b plots the possible Z_{ref} of the system of interest. Since both the power map and the Z_{ref} trajectory are plotted on a plane with the vertical and horizontal axes representing the real and imaginary parts of Z_{ref} it is possible to superimpose the two. Then, by reading the value of the power map at the point where the Z_{ref} trajectory is drawn, the amount of power that can be transferred in that state, can be determined.

In the example in Fig. 3, it can be seen that the larger the R_{ref}, the more power that can be transferred. In addition, the Z_{ref} trajectory is located to the left of 1,000W, indicating that it cannot transfer more than 1,000W.

The conventional impedance map shown in Fig. 3 considers only sine wave input and cannot evaluate efficiency. This study proposes a new impedance map that satisfies these requirements and aims to provide a more accurate understanding of the system.

III. THEORY OF THE IMPEDANCE MAP FOR EFFICIENCY

It is necessary to derive an expression for efficiency corresponding to the impedance map and to establish a method for synthesizing the conventional map and new efficiency map. First, how to derive the efficiency equation will be discussed. Usually, efficiency in an electric circuit can be derived by dividing the output power by the input power. Therefore, efficiency can be introduced into the impedance map by expressing input and output power in terms of Z_{ref}. Using the input voltages V_{in} and Z_{in}, the input power P_{in} can be expressed as in (5).

$$P_{in} = \frac{R_{in}}{R_{in}^2 + X_{in}^2} V_{in}^2 \tag{5}$$

From (5), if Z_{in} can be expressed in terms of Z_{ref}, the input power can be transformed into the appropriate form.

The output power can be considered in the same way as the input power; in Fig. 1, the output power P_{out} consumed by the load resistance can be expressed as in (6). In (6), Z_s can be expressed in terms of Z_{ref} by substituting into (1). V_{ind} can also be expressed in terms of Z_{ref} as in (7).

$$P_{out} = Z_{ac} \left(\frac{Z_5 V_{ind}}{Z_s (Z_5 + Z_6 + Z_{ac})} \right)^2 \tag{6}$$

$$V_{ind} = j\omega L_m \frac{V_{in}}{Z_{in}} \left(\frac{Z_2}{Z_2 + Z_3 + Z_{ref}} \right) \tag{7}$$

In the circuit shown in Fig. 1, R_{in} and X_{in}, the real and imaginary parts of the input impedance Z_{in}, can be expressed in terms of R_{ref} and X_{ref} the real and imaginary parts of Z_{ref} as in (8) and (9).

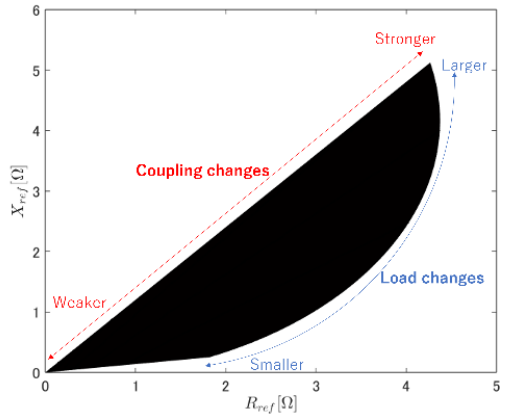

Fig. 4. Proposed Extended Z_{ref} Trajectory

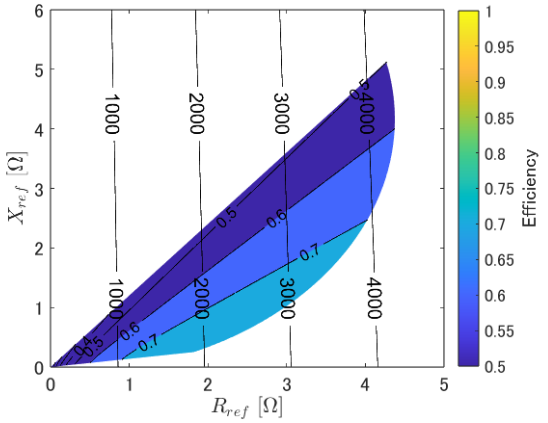

Fig. 5. Proposed Impedance Map

$$R_{in} = R_1 + \frac{(R_2+R_3+R_{ref})(R_2R_3+R_2R_{ref}-X_2X_3-X_2X_{ref})+(X_2+X_3+X_{ref})(X_2X_3+X_2X_{ref}+R_2X_3+R_2X_{ref})}{R_2^2+R_3^2+R_{ref}^2+2(R_2R_3+R_3R_{ref}+R_{ref}R_2)+X_2^2+X_3^2+X_{ref}^2+2(X_2X_3+X_3X_{ref}+X_{ref}X_2)} \quad (8)$$

$$X_{in} = X_1 + \frac{(R_2+R_3+R_{ref})(X_2R_3+X_2R_{ref}+R_2X_3+R_2X_{ref})+(X_2+X_3+X_{ref})(X_2X_3+X_2X_{ref}-R_2R_3-R_2R_{ref})}{R_2^2+R_3^2+R_{ref}^2+2(R_2R_3+R_3R_{ref}+R_{ref}R_2)+X_2^2+X_3^2+X_{ref}^2+2(X_2X_3+X_3X_{ref}+X_{ref}X_2)} \quad (9)$$

By using the power obtained using (5) ~ (9), the efficiency can be expressed in terms of Z_{ref}.

Next, the derived efficiency is used to create an efficiency map in a form that can be synthesized into a conventional impedance map. The conventional impedance map contains two types of data: transferable power and Z_{ref} trajectory, as shown in Fig. 2. Therefore, in order to add new elements while maintaining visibility, it is necessary to change the conventional impedance map into a form that can be combined with the efficiency map. Conventional impedance maps look at variations in either the coupling coefficient or load resistance only. Therefore, as shown in Fig. 2b, the Z_{ref} trajectory is a line shape. By calculating the Z_{ref} trajectory in such a way that the variation of both the coupling coefficient and load resistance are simultaneously taken into account, a plane Z_{ref} trajectory can be plotted as shown in Fig. 4. Fig. 4 assumes that the load resistance varies from 10 Ω to 100 Ω. The black area in Fig. 4 is the Z_{ref} trajectory and represents the operating range of Z_{ref}. As for the variation of the coupling coefficient, it was varied from 0.00319 to 0.124 as in Fig. 2b and Fig. 3.

Since the location of the Z_{ref} trajectory in relation to the power map is important to check for compatibility, additional elements can be added if they are on the trajectory. Since the objective of this study was to include an efficiency factor, an efficiency factor was added to the impedance map by superimposing an efficiency map over the trajectory as shown in Fig. 5.

In Fig. 5, values such as 1000 and 2000 represent transferable power, and values such as 0.7 represent the efficiency value that the WPT system of interest can take. In the proposed impedance map, the compatibility of power can be checked from the positional relationship between the lines on the power map and the efficiency map, and the compatibility of efficiency can be checked from the values on the efficiency map.

For example, assume that the system under consideration requires 1000W transfer power and an efficiency of at least 60%. Then in the example in Fig. 5, the efficiency map is to the left of the 1000W line, so the power aspects are not compatible, and reading the values on the efficiency map shows that there are areas below 60%, indicating that there is no compatibility on the efficiency side too.

From Fig. 5, it can be seen that the system in this paper has a small amount of power that can be transferred and is not capable of transferring the 20 kW required by the DWPT system. The problem of transferable power can be solved by increasing the diameter of the litz wire used in the transmitting and receiving coils and by improving the inverter. In Figure 5, a litz wire with a conductor outer diameter of 5.87 mm is used, resulting in a rated current of 38 A. However, a litz wire with a conductor outer diameter of 8.56 mm can carry a maximum current of 96 A. Also, the rated voltage of the inverter is set at 438 V, but 1100 V products for electric vehicles are expected. By relaxing the two constraints of the litz wire and the inverter, the power map changes as shown in Fig. 6a, indicating that it can handle higher power. Fig. 6b shows the proposal Impedance Map using Fig. 6a. The efficiency map of Fig. 6b is same as Fig. 5.

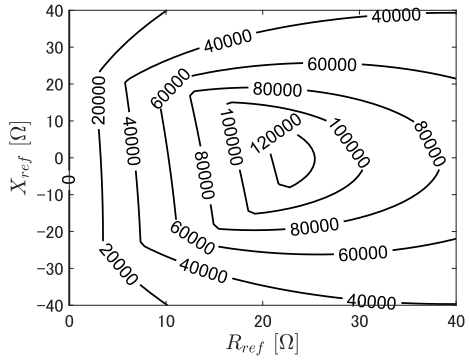

(a) Power map with relaxed constraints

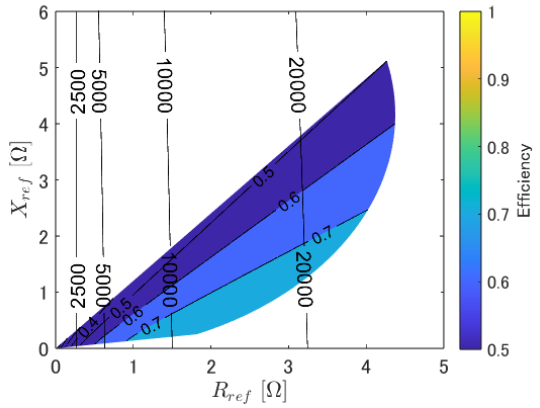

(b) Proposed Impedance Map using power map constraints in Fig.6a

Fig. 6. Allevation of power map constraints

From Fig. 6, the line cut out from the power map has been increased in power, but the efficiency map extends to the left end, indicating that the system in this paper is not capable of transferring the 20 kW required by the DWPT system. From Fig. 4, the efficiency map extends to the left as the coupling coefficient decreases. Therefore, by limiting the allowable misalignment, the system can handle high power for DWPT. When the maximum positional misalignment is reduced from 300 mm to 100 mm, the lowest coupling coefficient is 0.111. The proposed impedance map created using this parameter is shown in Fig. 7a.

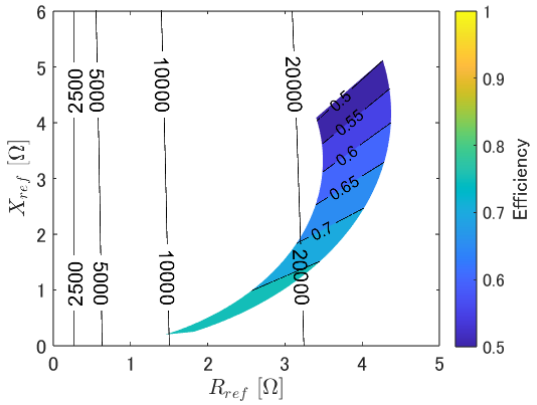

(a) coupling restrictions added to Fig.5

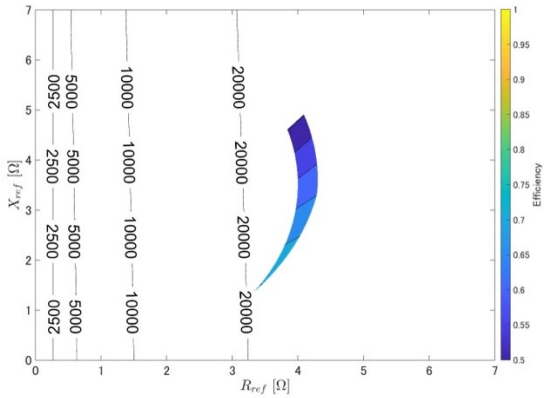

(b) added load limits to Fig6(a)

Fig. 7. Proposed Impedance Map by using parameters applicable to DWPT

From Fig. 7a, the efficiency map is to the right of the 10-kW line, indicating that more than 10 kW of transfer power is possible. In addition to Fig. 7a, consider the constraints of the SAE J2954 [18], the standard for supplying power to stationary vehicles. The J2954 test station requires the load voltage to be between 280V and 420V. Since the load voltage variation can be controlled by adjusting the load resistance variation, Fig. 7b shows a proposed impedance map with the load variation limited. In Fig. 7b, the load is calculated with the input voltage set to 500 V, which is the upper limit of CHAdeMO 1.0 [19], one of the most popular charging standards today. From the calculations, the load was varied between 24.1 Ω and 49.5 Ω in Fig. 7b. From Fig. 7b, the efficiency map is to the right of the 20-kW line, indicating that more than 20 kW of transfer power is possible, making it compatible in terms of power with the DWPT. Therefore, the parameters could be adjusted to those required for the 20-kW transfer power needed for the DWPT by using proposed impedance map.

Fig. 6 was calculated with a sine wave input. A sine wave input and the more commonly used square wave have similar characteristics, but a more realistic value can be obtained by taking a different approach. A square wave can be approximated as a set of 1st, 3rd, 5th, and more harmonics as (10). In (10), V_{in} represents the RMS of the input voltage, f represents the frequency of V_{in}, and t represents time.

$$V = V_{in}\sqrt{2}\sin(2\pi fnt) \tag{10}$$

$$V_{square} = \sum_{n=1}^{\infty} \frac{1}{2n-1} V \tag{11}$$

The impedance map corresponding to the square wave input can be drawn by using the proposed method based on (10) and (11) and synthesizing the obtained values.

IV. Measurement Results

The validity of the proposed method was confirmed by comparing the experimental values with those obtained by the impedance map calculations. Experiments were conducted using the same parameters as in Table I, as shown in Fig. 8. In this experiment, the coil shown in Fig. 9 was used. A square wave of approximately 50 V and 85 kHz was input as the power supply. Since the parameters are the same as in Table I, the proposed impedance map for the experimental system is the same as in Fig. 5.

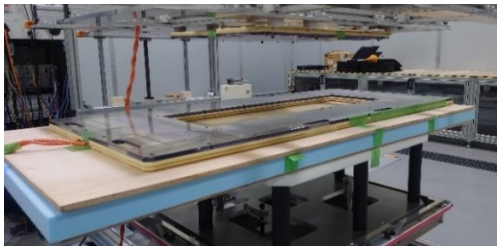

Fig. 8. Coil Layout of the Experiment

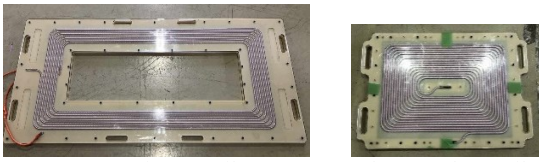

(a) Primary Coil (b) Secondary Coil

Fig. 9. Coils used in the Experiment

TABLE II. COIL MISALIGNMENT RANGE IN THE EXPERIMENT

	Width direction	Length direction	Height direction
Distance from center	0 to 300 mm	0 mm	250 mm

TABLE III. MISALIGNMENT AND COUPLING COEFFICIENTS

Width misalignment	0 mm	100 mm	150 mm	300 mm
Coupling coefficient	0.124	0.111	0.091	0.003

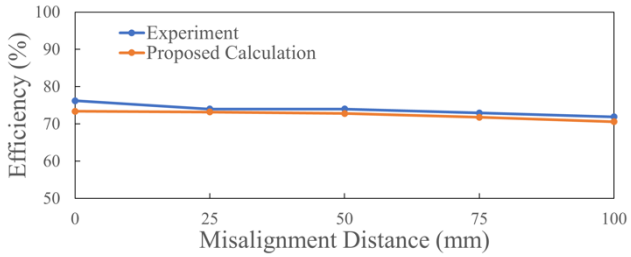

Fig. 10. Results of the Experiment

In the experiment, the coupling coefficient was first measured by shifting the position of the transmitting and receiving coils. The ranges of the positional displacements are shown in Table II. Next, power transfer was performed at each coil position and transfer characteristics were measured. In the ranges shown in Table I, the coupling coefficients varied as shown in Table III.

The efficiency values obtained from experiments and calculated by the proposed method are shown in Fig. 10.

From Fig. 10, the largest error was at the point with a misalignment distance of 0, where the error rate was 3.8 %. The resonant circuits of the experimental system, Z_3 and Z_4, have capacitor error rates of 10 % each, while Z_2 and Z_5 each have capacitor error rates of 4.9 %. Since the difference between the experimental and calculated values is smaller than these error rates, the experimental and calculated values can be said to match. From Fig. 10, the impedance map created by using the proposed method can be confirmed the validity.

From Figs. 5, 6 and 7, the efficiency is low for a magnetic field coupling system; a transfer efficiency of 80 % or higher is desirable. From reading the values on the efficiency map in Fig.7, it can be seen that even if constraints are added to limit the drawing range of the efficiency map, it is not possible to achieve an efficiency of 80 % or higher. In this case, it is necessary to change the circuit or system itself, rather than limiting positional deviation or load voltage. Looking at the circuit elements used in this experiment, it can be seen that Z_4, one of the resonant capacitors used in the experiment, has high internal resistance as shown in Table I and is one of the causes of poor efficiency. Therefore, the efficiency was improved when the internal resistance of Z_4 was set as 30.7 mΩ, a magnitude close to that of Z_3. By using this improved parameter, the efficiency exceeds 80 %. The proposed impedance map drawn by applying this improved parameter is shown in Fig.11.

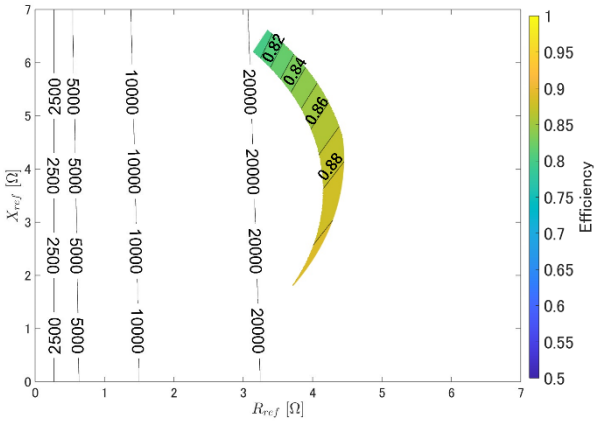

Fig. 11. Impedance Map with improved parameters

From Fig.11, the efficiency exceeds 80% in all areas on the efficiency map and the efficiency map is in the area over the 20,000 W line. By using the proposed impedance map, this WPT system was able to be improved and successfully achieve the desired value.

V. CONCLUSION

The analysis method was proposed. It can add efficiency to the impedance map, which is a method to understand transfer characteristics and to verify compatibility regarding power transfer. By using the proposed impedance map, compatibility can be verified even for systems where efficiency needs to be considered. The proposed impedance map was validated through experiments. The experimental system could be improved by using the proposed method. Therefore, the proposed impedance map allows us to consider the transfer characteristics corresponding to the misalignment of the transmitter and receiver coils more closely to the actual environment when designing a DWPT system, and to confirm compatibility.

ACKNOWLEDGMENT

This paper is based on results obtained from a project, JPNP21005, subsidized by the New Energy and Industrial Technology Development Organization (NEDO) in cooperation with DAIHEN Corporation.

REFERENCES

[1] A. Kurs, A. Karalis, R. Moffatt, J. D. Joannopoulos, P. Fisher, and M. Soljacic, “Wireless Power Transfer via Strongly Coupled Magnetic Resonances,” Science, Vol. 317, No. 5834, pp. 83-86, 2007.

[2] A. C. Bagchi, A. Kamineni, R. A. Zane and R. Carlson, "Review and Comparative Analysis of Topologies and Control Methods in Dynamic Wireless Charging of Electric Vehicles," in IEEE Journal of Emerging and Selected Topics in Power Electronics, vol. 9, no. 4, pp. 4947-4962, Aug. 2021.

[3] Z. Zhou, L. Zhang, Z. Liu, Q. Chen, R. Long and H. Su, "Model Predictive Control for the Receiving-Side DC–DC Converter of Dynamic Wireless Power Transfer," in IEEE Transactions on Power Electronics, vol. 35, no. 9, pp. 8985-8997, Sept. 2020.

[4] R. Tavakoli, T. Shabanian, E. M. Dede, C. Chou and Z. Pantic, "EV Misalignment Estimation in DWPT Systems Utilizing the Roadside Charging Pads," in IEEE Transactions on Transportation Electrification, vol. 8, no. 1, pp. 752-766, March 2022.

[5] A. N. Azad, A. Echols, V. A. Kulyukin, R. Zane and Z. Pantic, "Analysis, Optimization, and Demonstration of a Vehicular Detection System Intended for Dynamic Wireless Charging Applications," in IEEE Transactions on Transportation Electrification, vol. 5, no. 1, pp. 147-161, March 2019.

[6] R. Tavakoli and Z. Pantic, "Analysis, Design, and Demonstration of a 25- kW Dynamic Wireless Charging System for Roadway Electric Vehicles," in IEEE Journal of Emerging and Selected Topics in Power Electronics, vol. 6, no. 3, pp. 1378-1393, Sept. 2018.

[7] A. Mahesh, B. Chokkalingam and L. Mihet-Popa, "Inductive Wireless Power Transfer Charging for Electric Vehicles–A Review," in IEEE Access, vol. 9, pp. 137667-137713, 2021.

[8] S. Zou, O. C. Onar, V. Galigekere, J. Pries, G. -J. Su and A. Khaligh, "Secondary Active Rectifier Control Scheme for a Wireless Power Transfer System with Double-Sided LCC Compensation Topology," IECON 2018 - 44th Annual Conference of the IEEE Industrial Electronics Society, 2018, pp. 2145-2150.

[9] Y. Yamada, T. Imura and Y. Hori, "Theorizing a Simple Ferrite Cored Coil Using Image Coils in Wireless Power Transfer," in IEEE Access, vol. 11, pp. 8065-8072, 2023.

[10] J. Hou, Q. Chen, Z. Zhang, S. C. Wong, and C. K. Tse, “Analysis of Output Current Characteristics for Higher Order Primary Compensation in Inductive Power Transfer Systems,” IEEE Trans. Power Electron., vol. 33, no. 8, pp. 6807–6821, 2018.

[11] Kodai Takeda, Takehiro Imura, Toshiyuki Fujita, Takafumi Koseki and Yusuke Minagawa, "Visualized Evaluation of Feasibility of Power Transmission with Electrical Constraints in Wireless Power Transfer," 2020 IEEE PELS Workshop on Emerging Technologies; Wireless Power (WoW2020), Nov. 2020.

[12] Kodai Takeda, Toshiyuki Fujita, Takehiro Imura and Takafumi Koseki, “Power Transmission Characteristics of LCC Compensation Network to Coupling and Load Variation,” 5th International Electric Vehicle Technology Conference 2021, May 2021.

[13] Siqi Li, Weihan Li, Junjun Deng, Trong Duy Nguyen and Chunting Chris Mi, “A Double-Sided LCC Compensation Network and Its Tuning Method for Wireless Power Transfer,” IEEE Transactions on Vehicular Technology, VOL.64, NO.6, Jun 2015.

[14] Wei Zhang, Chunting Chris Mi,” Compensation Topologies of High-Power Wireless Power Transfer Systems,” IEEE Transactions on Vehicular Technology, VOL.65, NO.6 Jun 2016.

[15] Weihan Li, Han Zhao, Junjun Deng, Siqi Li, Chunting Chris Mi,” Comparison Study on SS and Double-Sided LCC Compensation Topologies for EV/PHEV Wireless Chargers,” IEEE Transactions on Vehicular Technology, Vol.65, NO.6, Jun 2016.

[16] Yuto Yamada Takehiro Imura, "An Efficiency Optimization Method of Static Wireless Power Transfer Coreless Coils for Electric Vehicles in the 85 kHz Band Using Numerical Analysis", IEEJ TRANSACTIONS ON ELECTRICAL AND ELECTRONIC ENGINEERING IEEJ Trans 2022, vol.17, Issue 10, pp. 1506-1516, October. 2022.

[17] Ryotetsu Sakurai, Takehiro Imura and Yoichi Hori, “Efficiency and Power Compatibility Visualization Methodology for Wireless Power Transfer,” IEE-SPC (in Japanease), Jun. 2022.

[18] SAE International, “Wireless Power Transfer for Light-Duty Plug-in/Electric Vehicles and Alignment Methodology J2954,” Issued2016-05, Revised2020-10.

[19] JIS D61851-23, Road vehicles -- Electrical receptacle for plug-in hybrid electric vehicles -- Part 23: Dimensional compatibility and safety requirements for a.c./d.c. pin and contact-tube accessories, 2014.